Micro- and Macrophase Separations of Hydrophobically Solvated Block Copolymer Aqueous Solutions Induced by Pressure and Temperature

Noboru Osaka,[†] Satoshi Okabe,[†] Takeshi Karino,[†] Yumi Hirabaru,[‡] Sadahito Aoshima,[‡] and Mitsuhiro Shibayama*,[†]

Neutron Science Laboratory, Institute for Solid State Physics, University of Tokyo, 106-1 Shirakata, Tokai, Ibaraki 319-1106, Japan, and Department of Macromolecular Science, Graduate School of Science, Osaka University, Toyonaka, Osaka 560-0043, Japan

Received March 31, 2006; Revised Manuscript Received June 23, 2006

ABSTRACT: The pressure- and temperature-induced micro- and macrophase separations of hydrophobically solvated block copolymer aqueous solutions, consisting of poly[2-(2-ethoxy)ethoxyethyl vinyl ether]-*block*-poly-(2-methoxyethyl vinyl ether) (pEOEOVE-*b*-pMOVE), have been investigated with dynamic light scattering (DLS) and small-angle neutron scattering (SANS). The following facts were disclosed. (1) For an increase in temperature under atmospheric pressure, a series of scattering peaks appeared in SANS intensity curves at about 40 °C, indicating microphase separation with pEOEOVE domains in a bcc packing in the matrix of pMOVE and water. This was followed by a precipitation of the polymer at about 65 °C. (2) A pressure−temperature ($P-T$) phase diagram for microphase separation was determined by DLS, which was a convex-upward function of P with a symmetric axis of $P_0 \approx 150$ MPa. (3) At ambient temperature, an increase of the correlation length was observed by increasing P. This was confirmed to be due to macrophase separation by pressurizing. (4) On the other hand, the solution underwent a reentrant microphase dissolution−separation transition at 45 °C with increasing P. The SANS peaks disappeared and the intensity decreased at 100 MPa. Then, by further increasing P, the SANS intensity increased accompanying a scattering maximum. In view of the symmetry of the phase diagram, it is conjectured that this reentrant microphase separation at high pressure is different from one at low pressure. These findings lead to a conclusion that the selectivity of hydrophobic solvation is suppressed at high pressures.

Introduction

A block copolymer consists of unlike linear polymer chains, which are connected at one end of each block chain by a covalent bond. Therefore, not a macrophase separation but a microphase separation is often observed in a block copolymer solution due to the connectivity and the difference in the affinity from the solvent. Such microphase separation sometimes leads to an ordered state, and a variety of unique periodic structures with nanometer scales such as lamella, cylinder, sphere structures, etc. are observed.[1−3]

There are a lot of reports on pressure-dependent microphase separation of block copolymers. However, most of these works were on the pressure dependence of the Flory interaction parameter,[4−6] order−disorder transition,[5] order−order transition, and/or the pressure dependence of the polymer conformation.[4] Schwahn et al. observed an abnormal pressure dependence of the phase boundary of poly(ethylethylene)/poly(dimethylsiloxane) block copolymers.[6] They explained this with a dominating increase in the entropic Flory−Huggins parameter. On the other hand, to our knowledge, there have been only a few papers which dealt with pressure-induced microphase separation of block copolymer aqueous solutions. It is known that water molecules surrounding hydrophobic groups favor to form an ordered structure, i.e., the so-called iceberg, with a penalty being a loss of entropy.[7−9] External parameters such as heat, solvent, and light etc. could destroy the iceberg structure, resulting in destabilization of the system. Since pressurization increases the density of the system without changing the thermal energy of the molecules, it is considered that pressure directly influences such an iceberg structure. Furthermore, the employment of block copolymer aqueous solutions is more advantageous to investigate the nature of hydrophobic solvation since the molecular interactions among the constituent block chains and solvent can be studied in terms of microphase separation behavior and the resultant microdomain structures.

The phase behavior of aqueous polymer solutions and gels by pressurizing were extensively investigated for poly(*N*-isopropylacrylamide) (PNIPA),[10] and weakly charged copolymers, e.g., poly(*N*-isopropylacrylamide-*co*-acrylic acid).[11,12] A convex-upward $P-T$ phase separation curve was observed for both of the hydrophobically solvated polymer systems. Also, a reentrant phase behavior by pressurizing at high temperature was detected. Such distinct phase behavior was qualitatively explained in the view of hydrophobic solvation. In the previous paper, we discussed various phase behaviors of block copolymer aqueous solutions of an amphiphilic block copolymer, poly(2-(2-ethoxy)ethoxyethyl vinyl ether)-*block*-poly(2-methoxyethyl vinyl ether) (pEOEOVE-*b*-pMOVE), from the viewpoint of hydrophobic solvation.[13] In this paper, we begin with the determination of the phase diagram based on dynamic light scattering (DLS) data and look into the phase behaviors of the same system more deeply for a better understanding of hydrophobic solvation at elevated pressures.

Theoretical Background

DLS. DLS can be used to analyze the dynamics of polymer solutions. The correlation function, $g^{(1)}(\vec{q},\tau)$, for the scattered

* Corresponding author. E-mail: shibayama@issp.u-tokyo.ac.jp.
[†] Neutron Science Laboratory, Institute for Solid State Physics, University of Tokyo.
[‡] Department of Macromolecular Science, Graduate School of Science, Osaka University.

10.1021/ma060723o CCC: $33.50
Published on Web 07/26/2006

electric field from the sample, is defined by

$$g^{(1)}(\vec{q},\tau) \equiv \frac{\langle E(\vec{q},0)E^*(\vec{q},\tau)\rangle}{\langle E(\vec{q},0)\rangle^2} \quad (1)$$

where $\vec{q}$, τ, and $E(\vec{q},\tau)$ are the scattering vector, the decay time, and the scattering field, respectively. Here, $\langle\cdots\rangle$ indicates a time or an ensemble averaging. In a DLS measurement, we obtain the second-order correlation function, $g^{(2)}(\vec{q},\tau)$, which is the intensity−intensity−time correlation function defined by

$$g^{(2)}(\vec{q},\tau) \equiv \frac{\langle I(\vec{q},0)I(\vec{q},\tau)\rangle}{\langle I(\vec{q},0)\rangle^2} = \frac{\langle E(\vec{q},0)E^*(\vec{q},0)E(\vec{q},\tau)E^*(\vec{q},\tau)\rangle}{\langle |E(\vec{q},0)|^2\rangle^2} \quad (2)$$

Here, $I(\vec{q},\tau)$ is the scattered intensity at $\vec{q}$ and at time τ.

In the case of an ergodic medium, where time averaging is equal to ensemble averaging, the scattered electric field obeys the Gaussian distribution, and then, the above two correlation functions are linked via the Siegert relation,[14]

$$g^{(2)}(\vec{q},\tau) = 1 + |g^{(1)}(\vec{q},\tau)|^2 \quad (3)$$

In an ideal case of an ergodic system, $g^{(2)}(\vec{q},\tau) - 1$ approaches 1 at $\tau = 0$.

On the other hand, in the case of nonergodic medium, the scattered electric field, $E(\vec{q},\tau)$, is decomposed into the two scattered fields components by the time-constant static fluctuation, $E_C(\vec{q})$, and the time-dependent dynamic fluctuations, $E_F(\vec{q},\tau)$, and we can write

$$E(\vec{q},t) = E_C(\vec{q}) + E_F(\vec{q},t) \quad (4)$$

By substitution of eq 4 into eq 2, $g^{(2)}(\vec{q},\tau)$ is written as

$$g^{(2)}(\vec{q},\tau) \equiv \frac{\langle I(\vec{q},0)I(\vec{q},\tau)\rangle_T}{\langle I(\vec{q},0)\rangle_T^2} = 1 + X^2 g_F^{(1)}(\vec{q},t)^2 + 2X(1-X)g_F^{(1)}(\vec{q},t) \quad (5)$$

where $\langle\cdots\rangle_T$ denotes time averaging. Here, X and $g_F^{(1)}(\vec{q},t)$ are the ratio of the fluctuating intensity to the total intensity and the intermediate correlation function associated with the dynamic scattering component, respectively, which are defined by

$$X = \frac{\langle I_F\rangle_T}{\langle I\rangle_T} \quad (6)$$

$$g_F^{(1)}(\vec{q},\tau) \equiv \frac{\langle E_F(\vec{q},0)E_F^*(\vec{q},\tau)\rangle}{\langle I_F(\vec{q},0)\rangle} \quad (7)$$

Note that the initial value of $g^{(2)}(\vec{q},\tau) - 1$ for a nonergodic system ($X \neq 0$) always remains below 1. Following the above discussion, it is shown that the initial value of $g^{(2)}(\vec{q},\tau) - 1$ can be used to determine an ergode-nonergode transition. $g^{(1)}(q,\tau)$ is related to the decay rate distribution function, $G(\Gamma)$, via Laplace transform as is given by

$$g^{(1)}(\vec{q},\tau) = \int_0^\infty G(\Gamma)\exp(-\Gamma\tau)\,d\Gamma \quad (8)$$

where Γ is the decay rate. It is known that $G(\Gamma)$ generally becomes broad at the gelation threshold.[15]

SANS Intensity function for Polymer Solutions

(1) Ornstein−Zernike Function. For a polymer solution in semidilute regime, the correlation length ξ, i.e., a characteristic length of concentration fluctuation, can be evaluated with the following Ornstein−Zernike (OZ) equation:

$$I_{OZ}(q) = \frac{I_{OZ}(0)}{1 + q^2\xi^2} \quad (9)$$

where $I_{OZ}(0)$ and ξ are the scattering intensity at $q = 0$ and the correlation length, respectively. The details of this function is described elsewhere.[16]

(2) Hosemann's Paracrystal Theory. Block copolymers undergo microphase separation even if they are in a solvent. In particular, if the solvent is selective to one component of the block copolymer, a well-developed microdomain structure is formed due to a selective solvation of the like-block chains and micellization of the unlike block chains.[17] This type of microphase-separated structure leads to an appearance of a series of peaks in small-angle X-ray or neutron scattering curves. The paracrystal theory was developed to describe the three-dimensional structure of the macrolattice.[18] The scattering intensity function consists of two parts, namely the form factor for noninterfering spherical particles, $P(q)$, and the lattice factor, $Z(q)$. The theoretical function is the multiplication of the two functions and is expressed as

$$I(q) = P(q)Z(q) \quad (10)$$

The spherical form factor is

$$P(q) = nV^2\Delta\rho^2\Phi^2(qR) \quad (11)$$

$$\Phi(qR) = \frac{3[\sin(qR) - qR\times\cos(qR)]}{(qR)^3} \equiv \sqrt{\frac{\pi}{2}}\frac{J_{3/2}(qR)}{(qR)^{3/2}} \quad (12)$$

where n is the number density of the spheres, $\Delta\rho^2$ is the square of the difference in the scattering length densities between a spherical particle and a matrix, R is the radius of the sphere, and V is the volume of the sphere. $Z(q)$ is obtained by multiplying $Z_k(q)$ for $k = 1,2$, and 3 (k is the axis number in the three-dimensional rectangular coordinate.) and then integrating for all the possible orientations.

$$Z_K(q) = \frac{1 - |F(q)|^2}{1 - 2|F(q)|\cos^2(\vec{a}_k\cdot\vec{q}) + |F(q)|^2} \quad (13)$$

where $F(q)$ is the factor relating the degree of distortion

$$|F(q)| = \exp\left[-\frac{1}{2}\frac{\Delta a^2}{a^2}\{(\vec{a}_1\cdot\vec{q})^2 + (\vec{a}_2\cdot\vec{q})^2 + (\vec{a}_3\cdot\vec{q})^2\}\right] \quad (14)$$

where a and Δa are the unit cell distance and its standard deviation, assuming isotropic distortions, respectively. The ratio $g \equiv \Delta a/a$ is often called the Hosemann's g-factor, which determines the degree of paracrystallinity. Here, $\vec{a}_1$, $\vec{a}_2$ and $\vec{a}_3$ are the unit vectors of the principal axes assuming a body-centered cubic (bcc) structure.

Experimental Section

Samples. Poly[2-(2-ethoxy)ethoxyethyl vinyl ether]-*block*-poly(2-methoxyethyl vinyl ether), pEOEOVE-*b*-pMOVE, with a narrow

molecular weight distribution ($M_n = 5.7 \times 10^4$, $M_w/M_n = 1.28$) was synthesized by living cationic polymerization. The degrees of polymerization of each block were 200 and 400 for pEOEOVE and pMOVE, respectively. Both polymers have lower critical solution temperatures (LCST) at ca. 40 and ca. 65 °C, respectively for pEOEOVE and pMOVE. The polymerization was carried out at 0 °C under a dry nitrogen atmosphere in a glass tube equipped with a three-way stopcock baked at 250 °C for 10 min before use. The details of the synthesis were reported in a recent paper by Sugihara et al.[19] A prescribed amount of pEOEOVE-*b*-pMOVE was dissolved in deuterated water (D_2O). It should be noted that there exists a significant isotope effect in phase behavior in polymer solution.[20] Therefore, D_2O instead of H_2O was chosen as a solvent also for dynamic light scattering measurement (DLS) in addition to SANS experiments.

Differential Scanning Calorimetry (DSC). DSC measurements were carried out with a DSC8230 (Rigaku Co. Ltd.) at ambient pressure condition. The polymer concentrations were 5−20 wt %. The polymer solution was crimped in a sealed pan, and DSC thermograms were taken with a heating rate of 5 °C/min. The temperature range was 15−80 °C. No noticeable change in the weight of the sample pan before and after a DSC run was detected, indicating no water evaporation took place during the DSC run.

DLS. DLS experiments were conducted with a static/dynamic compact goniometer (SLS/DLS-5000), ALV, Langen, Germany. A He−Ne laser with a power of 22 mW (wavelength, $\lambda_L = 6328$ Å) was used as an incident beam. The decay time distribution functions $G(\Gamma)$ were calculated from the intensity−intensity−time correlation function, $g^{(2)}(\tau)$, using CONTIN data analysis package.[21] Pressure dependent DLS experiments were carried out with an inner-cell type pressure cell having a set of optical windows, PCI-400, Teramex, Co. Ltd. Kyoto, Japan.[22] The scattering angle was fixed to be 90°. The temperature of the sample was regulated by circulating water from a NESLAB RTE-111 thermocontroller with a precision of ±0.1 °C.

SANS. Pressure-dependent SANS experiments were carried out for 15 wt % pEOEOVE-*b*-pMOVE deuterated water solutions at SANS-U, the University of Tokyo, installed at JRR-3M reactor guide hall, the Japan Atomic Energy Agency.[23] The wavelength of the neutrons was monochromatized to be $\lambda = 7.0$Å with a mechanical velocity selector. The wavelength distribution, $\Delta\lambda/\lambda$, was 10%. The sample-to-detector distances were 2.00 and 8.00m, which provided the experimental q range to be from 0.006 to 0.2 Å^{-1}. Pressure-dependent SANS experiments were conducted with a pressure chamber, PCI-400-SANS, Teramex, Co. Ltd. Kyoto, Japan. The applied pressure was transmitted via a rubber diaphragm connected to the inner cell made of aluminum with quartz and sapphire windows. The sample thickness was 2.0 mm. The outer chamber was filled with D_2O and the pressure was controlled by pressurizing D_2O by a double-cylinder hand pump. The SANS measurements were conducted at $T = 28$, 40, 45, and 50 °C. The temperature of the sample was regulated by circulating water with the precision of ± 0.1 °C. Corrections for transmission, air and cell scattering were made before normalizing to the absolute intensity. For the absolute intensity calibration a polyethylene slab (Lupolen) sample was used.[24] After the absolute intensity calculation, incoherent scattering correction was made with the method reported by Shibayama.[24]

Results and Discussion

1. DSC. Phase separation temperatures of pEOEOVE-*b*-pMOVE aqueous solutions of various concentrations (5−20 wt %) at ambient pressure were determined with DSC at various heating rates (1.0−5.0 °C/min). A representative thermogram for a 15 wt % sample is shown in Figure 1a. The heating rate was 5 °C/min. As shown in the figure, two endotherms were clearly observed, which indicate a two-step phase separation at about 41 and 67 °C. The observed phase separation temperatures are close enough to those of the homopolymers, i.e., pEOEOVE (41 °C) and pMOVE (67 °C) aqueous solutions determined by light-transmittance measurements.[19] Hence, the two endothermic peaks were ascribed to the melting of iceberg structure of each segment. The enthalpy for hydrophobic dissociation for the 15 wt % solution was −3.435 J/g. This value corresponds to $\Delta H = -2.00$ kcal/mol per EOEOVE monomer. The value of ΔH for PNIPA is $\Delta H_{NIPA} = -0.946$ kcal/mol.[25−27] This distinction means that an EOEOVE monomer needs more water molecules to form an iceberg structure than that of PNIPA. Figure 1b shows photographs for a 15 wt % pEOEOVE-*b*-pMOVE solution taken at 20, 45, and 68 °C under atmospheric pressure. At 20 °C, the block copolymer molecules are dispersed in D_2O and the solution is transparent. However, the solution becomes hazy at 45 °C. At 68 °C, a precipitation was clearly observed. These changes in the appearance are well correlated with the observation of endothermic peaks. As will be verified later, the first endothermic peak can be assigned to microphase separation, while the latter to macrophase separation.

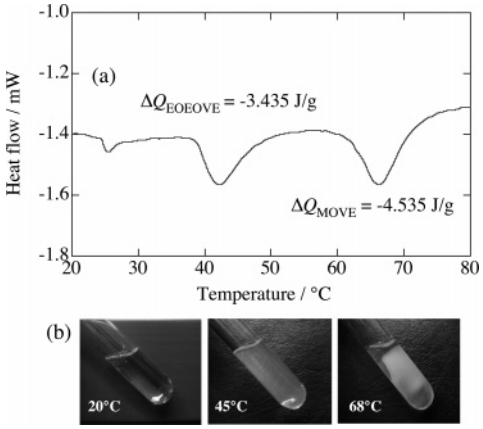

Figure 1. (a) DSC thermograms for 15 wt % pEOEOVE-*b*-pMOVE in D_2O and (b) photographs of the block copolymer solution in a test tube taken at 20, 45, and 68 °C.

2. DLS at Various Temperatures and Pressures. 2.1. *P*—*T* Phase Diagrams of pEOEOVE and of pMOVE. Although macroscopic separation is easily detected by a turbidity measurement and/or visual observation, the onset of microphase separation cannot be determined by these methods in principle. Hence, we conjecture that the appearance of this turbidity observed in this study indicates formation of giant micelles consisting of aggregated domains in addition to microphase separation. It should be noted here the following. The fraction of these giant micelles is not necessary to be large since a giant micelle scatters light much stronger than small ones due to the fact the scattering intensity being proportional to the sixth power of the micelle size. Another possibility is scattering from large grains having different orientations, where the grains consist of a finite size of macrolattice (i.e., a microdomain structure). Assuming that the major component is microphase-separated domains of pEOEOVE in the matrix of pMOVE and water, we tried to relate the DLS results with the thermal behaviors.

Figure 2 shows (a) the intensity−intensity−time correlation functions, $g^{(2)}(\tau) - 1$ and (b) the decay-rate distribution as a function of characteristic decay time, $G(\Gamma)$, for a 15 wt % pEOEOVE-*b*-pMOVE aqueous solution during the heating process at 0.1 MPa. Two interesting features can be drawn from this figure. (1) There is a characteristic decay time at around $\tau \approx 30$ ms, which shifts to the smaller decay time at the beginning and then shifts to the larger decay time with T. This characteristic decay may be assigned to disentanglement of transient network[28] or reptative motion, i.e., the slowest relaxation.[29] Recently, Yuan et al. reported that both homopolymer solutions

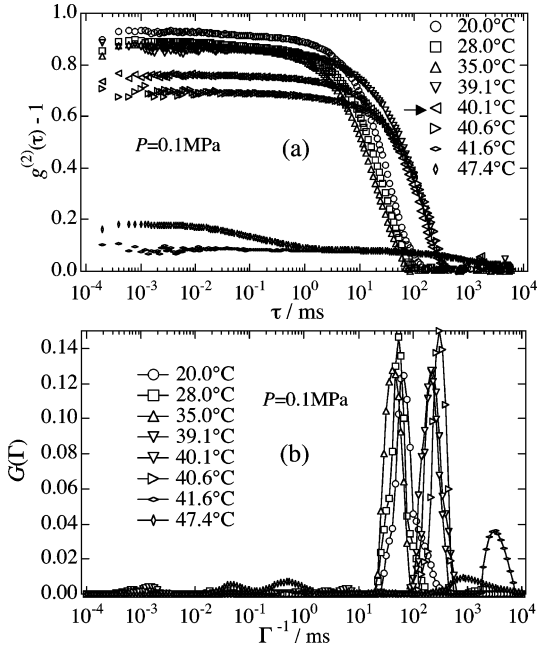

Figure 2. (a) Intensity−intensity−time correlation functions, $[g^{(2)}(\tau) - 1]$'s and (b) the decay rate distribution functions, $G(\Gamma)$'s, for 15 wt % pEOEOVE-*b*-pMOVE in D_2O, observed at various temperatures at 0.1 MPa.

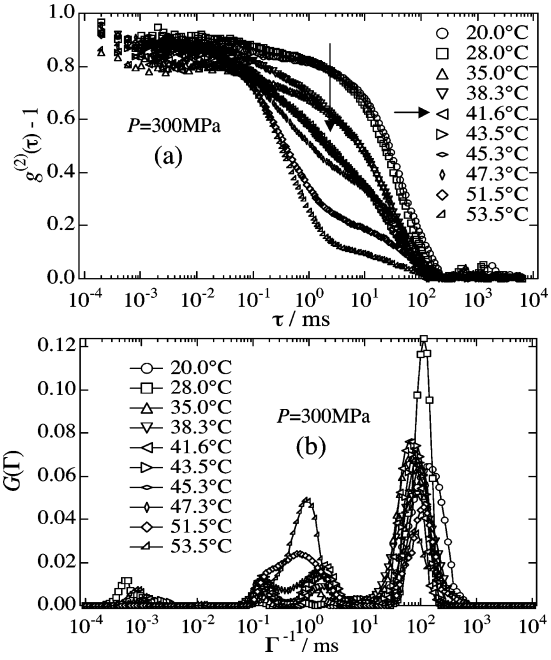

Figure 3. (a) $[g^{(2)}(\tau) - 1]$'s and (b) $G(\Gamma)$'s for 15 wt % pEOEOVE-*b*-pMOVE in D_2O, observed at various temperatures at 300 MPa.

and block copolymer solutions have a slow mode originating from the same physical picture, i.e., long-range concentration fluctuations of correlated polymer chains in transient network.[30] On the other hand, the so-called gel mode is not observable in this system. This is because the polymer concentration was much larger than the case where a gel mode can be resolved. This issue will be addressed in section 3.2. (2) A lowering of the initial value ($\tau = 0$) of $g^{(2)}(\tau) - 1$, σ_I^2, is observed, especially at around 40 °C (marked with an arrow). The small-τ shift is ascribed to a decrease in the viscosity of the solvent, i.e., water. However, the large-τ shift is deduced to be a result of micellization followed by physical gelation. This conjecture is examined by an observation of the suppression of the σ_I^2 since it is due to nonergodic nature of the system. In addition, transmission measurements on pEOEOVE-*b*-pMOVE aqueous solutions at $P = 0.1$ MPa exhibited a two-step decrease in the transmittance, indicating microphase separation as well as precipitation.[19] As mentioned above, a pEOEOVE-*b*-pMOVE aqueous solution forms a bcc-lattice structure with spherical micelles at nearly 40 °C under atmospheric pressure, which indicates a gelation of the system.[3,31] Thus, we conclude that this decrease of σ_I^2 is the onset of microphase separation at ambient pressure.

Figure 3 shows (a) $g^{(2)}(\tau) - 1$ and (b) $G(\Gamma)$ of a pEOEOVE-*b*-pMOVE aqueous solution during a heating process at 300 MPa. It should be noted that there is a marked difference in the DLS behaviors between 0.1 and 300 MPa. First of all, no decrease in σ_I^2 is detected during temperature scan, which made it difficult to determine a phase separation temperature. This *T*-independence means no gelation. However, as shown in Figure 3a, $g^{(2)}(\tau) - 1$ gradually changed with *T*. That is, the shoulder shifted to the faster decay time with *T*, and a new peak clearly appeared around $\tau = 1$ ms. We conjecture that this peak is due to the so-called gel mode. As will be discussed later in conjunction with SANS results, the correlation length increases with increasing *T* at $P = 300$ MPa, resulting in acquisition of gel mode. Hence, this relaxation mode is related to a different kind of microphase separation. However, we do not have further information about the structure, and we reserve its elucidation for future investigation.

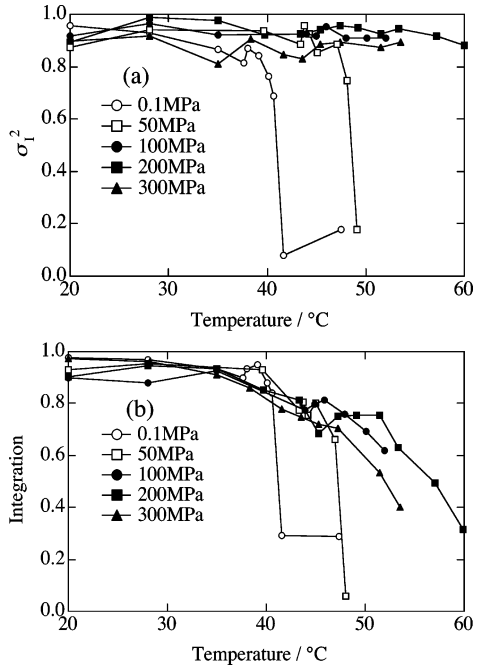

Figure 4. Temperature dependence of (a) the initial value of $[g^{(2)}(\tau) - 1]$, σ_I^2, (b) the integration value of the peak of the decay rate distribution function at 0.1, 50, 100, 200, and 300 MPa.

Figure 4 shows the temperature variations of (a) σ_I^2 and (b) integration of the peak of $G(\Gamma)$ for the solution at various pressures. Here, two types of interesting features are observed in σ_I^2, i.e., (1) a discrete suppression for $P \leq 50$ MPa and (2) a continuous decrease for 50 MPa $< P$. It is clear that the discrete change is corresponding to an ergode-nonergode transition. Hence, it means a gelation. On the other hand, the invariance of σ_I^2 for 50 MPa $< P$ indicates that the system remains in an ergodic medium, while $G(\Gamma)$ clearly indicates an appearance of a fast mode ($\tau \approx 1$ ms). At low temperatures, the relaxation corresponds to the slow mode (disentanglement

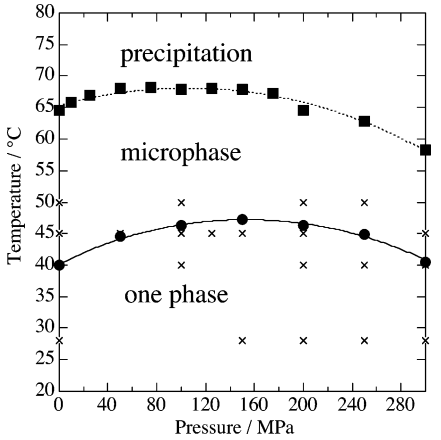

Figure 5. Phase diagram of 15 wt % pEOEOVE-*b*-pMOVE in D_2O. The solid line with filled circles indicate the microphase separation transition curve; the dotted line with solid squares denotes precipitation. The SANS measured points in the phase diagram are indicated with crosses.

of transient network).[32] Above the microphase separation temperature, all of the polymer-chain motions are arrested by microdomains followed by gelation. This is the case at ambient pressure. However, by increasing pressure, such a microphase separation becomes difficult and an ill-developed domain structure may be formed. These domains are not so strong to tie neighboring domains. Therefore, the system remains in an ergodic medium and a gellike mode (the fast mode) is preferentially observed. Since both features are related to microphase separation (or microdomain formation), we assigned both of these changes to the onset of microphase separation, i.e., a discrete suppression of the initial amplitude (for $P \leq 50$ MPa) and an appearance of a fast peak in $G(\Gamma)$ (for $P > 50$ MPa).

The phase diagram for 15 wt % pEOEOVE-*b*-pMOVE was constructed. The cloud point curve was determined by visual observation, which is shown by the dotted line in Figure 5. This corresponds to demixing of pMOVE chains. Note that pMOVE plays as an emulsifier below this temperature, but it precipitates above this temperature. This cloud point curve was reproducible and reversible with respect to both temperature and pressure. On the other hand, the microphase separation curve is vague in comparison with the precipitation curve. As will be shown below, SANS results solve this problem.

2.2. Thermodynamic Origin of the Upward-Convex *P*—*T* Phase Diagram. In this section, we discuss the origin of the phase behavior from thermodynamic points of view. A $P-T$ phase diagram of aqueous solutions are often represented with a parabolic function or an elliptic function.[10,33−35] The reason for convexity for a parabolic function is mainly ascribed to the pressure dependence of the compressibility of the components as described elsewhere.[11] In 1972, Hawley proposed an elliptic function for $P-T$ phase diagrams to describe nature-denature transition of proteins.[33] He started from the assumption that there are only two distinct states of the protein (native and denatured) and the transition between them is a two-state process. According to Hawley,[33] the Gibbs free energy difference ΔG between these states is defined as

$$\Delta G = \Delta G_{\text{denatured}} - \Delta G_{\text{native}} \tag{15}$$

By taking the total differentiation of ΔG, one obtains

$$\mathrm{d}\Delta G = -\Delta S\,\mathrm{d}T + \Delta V\,\mathrm{d}P \tag{16}$$

Upon integration of this equation from an arbitrarily chosen reference point (P_0, T_0) to (P, T), one obtains

$$\Delta G = \frac{V_0\Delta\beta}{2}(p-p_0)^2 + V_0\Delta\alpha(p-p_0)(T-T_0) - \Delta C_p\left[T\left(\ln\frac{T}{T_0}-1\right)+T_0\right] + \Delta V_0(p-p_0) - \Delta S_0(T-T_0) + \Delta G_0 \tag{17}$$

Here, β is the compressibility, V_0 is the volume at the reference state, α is the thermal expansivity factor, and C_p is the heat capacity. In the vicinity of the reference point, one can approximate

$$T\left(\ln\frac{T}{T_0}-1\right)+T_0 \cong \frac{(T-T_0)^2}{2T_0} \tag{18}$$

Hence, one gets,

$$\Delta G = \frac{V_0\Delta\beta}{2}(p-p_0)^2 + V_0\Delta\alpha(p-p_0)(T-T_0) - \Delta C_p\frac{(T-T_0)^2}{2T_0} + \Delta V_0(p-p_0) - \Delta S_0(T-T_0) + \Delta G_0 \tag{19}$$

The transition line, where the protein denatures, is defined by $\Delta G = 0$. Mathematically, this gives either a hyperbola or an ellipse. In really, it was found to be always elliptic for proteins. The characteristic feature of the elliptical phase diagram is discussed by Smeller.[34] As a result of the fitting, the following equations were obtained for pEOEOVE and pMOVE block copolymers in D_2O,

$$0.0336(P - 153.3\ \text{MPa})^2 + (T + 12.3\ ^\circ\text{C})^2 = 3536 \tag{20}$$

$$0.04(P - 104.6\ \text{MPa})^2 + (T + 12.7\ ^\circ\text{C})^2 = 6534 \tag{21}$$

where (P_0, T_0) = (153.3 MPa, −12.3 °C) and (P_0, T_0) = (104.6 MPa, −12.7 °C) are the centers of ellipses, respectively for pEOEOVE and pMOVE block chains in D_2O. Evaluations of the thermodynamic parameters, such as $\Delta\beta_0$ and ΔC_P, are beyond the scope of this paper since we do not have the information about the absolute value of ΔG. The significance of the success of the fitting is (1) to show that the phase diagram is rather symmetric with respect to P_0 and (2) to indicate the possibility of a phase separation of pEOEOVE-*b*-pMOVE by decreasing temperature. Regarding elliptic phase diagram, it is often obtained in the case of some proteins and synthetic polymers in which the mechanism of the phase separation is mainly derived from the scheme of hydration and dehydration of water. Thus, it is worthy to demonstrate that the phase diagram can be elliptic in the case of microphase separation of hydrated block copolymers as in the case of proteins.

3. Scattering Intensity Functions at Various Pressures and Temperatures. 3.1. Temperature Dependence at 0.1 MPa by SANS. SANS profiles for pEOEOVE-*b*-pMOVE at various temperatures at 0.1 MPa are shown in Figure 6. The SANS curve at 28 °C was well fitted with the OZ function as shown with the solid line, from which $I_{OZ}(0)$ and ξ were evaluated. It is noteworthy that the deviation of the observed $I(q)$ from the fit in the low q-region is due to nonequilibrium structure introduced at the stage of sample loading. Thus, it can be concluded that pEOEOVE-*b*-pMOVE chains are molecularly dispersed in water at 28 °C. At 40 °C, on the other hand, the intensity increased and a scattering maximum appeared (arrows).

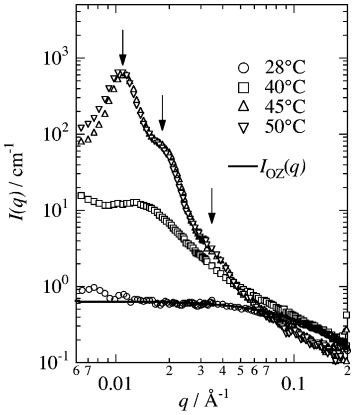

Figure 6. Scattering intensity functions, *I(q)s*, for pEOEOVE-*b*-pMOVE in D_2O with different temperatures. A thick line shows the result of curve fitting with an OZ function. Note that the deviation in *I(q)* for 28 °C at the low *q* region is due to nonequilibrium structure introduced at the stage of sample loading.

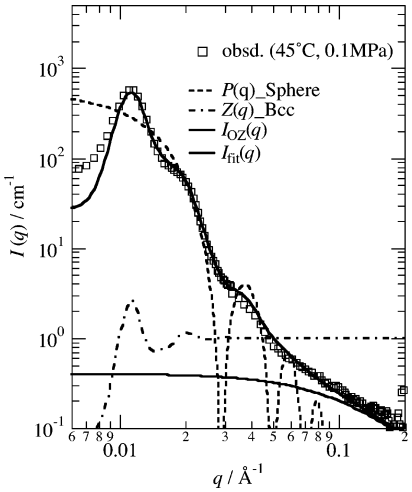

Figure 7. Results of curve fitting for pEOEOVE-*b*-pMOVE in D_2O at 0.1 MPa. Key: $P(q)$, the form factor; $Z(q)$, the lattice factor; $I(q)_{OZ}$, the OZ function; $I(q)_{fit}$, the fitted curve with a size distribution of spheres and instrumental smearing.

As clearly shown in Figure 7, the SANS profile at 45 °C clearly shows a series of peaks. To analyze the SANS intensity functions, we performed a curve fitting using the three-dimensional paracrystal theory discussed in Theoretical section. Similarly to the treatment in the previous papers,[31,36,37] the fitting function is the multiplication of the two functions in addition to the contribution of scattering from the matrix, and is expressed as

$$I(q) = P(q)Z(q) + I_{OZ}(q) \tag{22}$$

where the first and second terms of the RHS represent the scattered intensities for spherical domains and for semidilute solutions (i.e., the OZ function), respectively. Here, we also took into account of smearing effect due to a finite wavelength distribution in addition to collimation smearing. Note that the effect of the wavelength distribution becomes larger with increasing *q* due to the following relationship,

$$\mathrm{d}q = -\frac{4\pi}{\lambda^2}\sin\theta\,\mathrm{d}\lambda = -q\frac{\mathrm{d}\lambda}{\lambda} \tag{23}$$

The wavelength distribution was assumed to be a Gaussian function and the theoretical scattering function was smeared with the wavelength distribution function so as to reproduce the observed curve. The detail of the curve fitting is described elsewhere.[37] The result of the curve fitting for 45 °C at 0.1 MPa is displayed with the solid line. The fitted curve designated by the thick solid line well reproduces the observed scattering function. The radius of the sphere, *R*, and the lattice interval, *a*, are 155 and 775 Å, respectively. Their deviations $\Delta R/R$ and $\Delta a/a$ are 0.16 and 0.12, respectively. These values are comparable to those obtained in similar systems.[31,36] Hence, the model, i.e., spherical domains embedded in a polymer solution, seems to be reasonable. The SANS profile at 50 °C is quite similar to the curve at 45 °C. Thus, in the microphase-separated region at atmospheric pressure, the pEOEOVE-*b*-pMOVE forms clear microphase separation where the micelles are arranged in a bcc lattice packing. This result means that the selective solvation of block copolymer works well at ambient pressure.

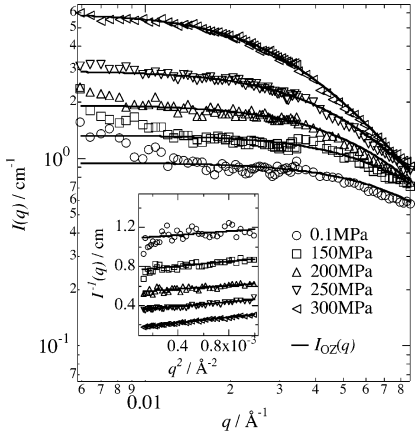

Figure 8. (a) Various SANS intensity functions, *I*(*q*)s, of pEOEOVE-*b*-pMOVE in D_2O by pressurizing at 28 °C. The solid lines in the inset denote results of curve fitting with OZ function. (b) Inverse *I*(*q*) vs q^2 plots. Note that the deviation in *I(q)* for 28 °C at the low *q* region is due to nonequilibrium structure introduced at the stage of sample loading.

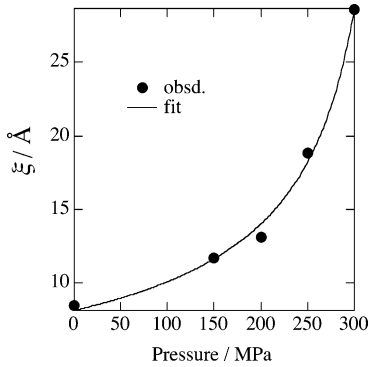

Figure 9. Pressure dependence of the correlation length at 28 °C.

3.2. Pressure Dependence at Low Temperature (28 °C). SANS profiles for 15 wt % pEOEOVE-*b*-pMOVE aqueous solutions at 28 °C at various pressures are shown in Figure 8. All of the curves are successfully fitted with the OZ equation (eq 9) as shown with the solid lines. As already mentioned above, the deviation at low *q*'s for the data at $P = 0.1$ MPa is due to frozen inhomogeneities. The inset shows *I*(*q*) vs q^2 plot, from which the susceptibility *I*(0) and the correlation length ξ were evaluated as a function of *P*. Thus, the block copolymers in aqueous solutions remained molecularly dispersed in these pressures without any specific interaction between the block chains. Figure 9 shows the pressure dependence of ξ at 28 °C. ξ was an increasing function of *P*. It is noted that this behavior does not agree to the "symmetry" of the phase separation curve with respect to $P = P_0$. The behavior of ξ seems to diverge

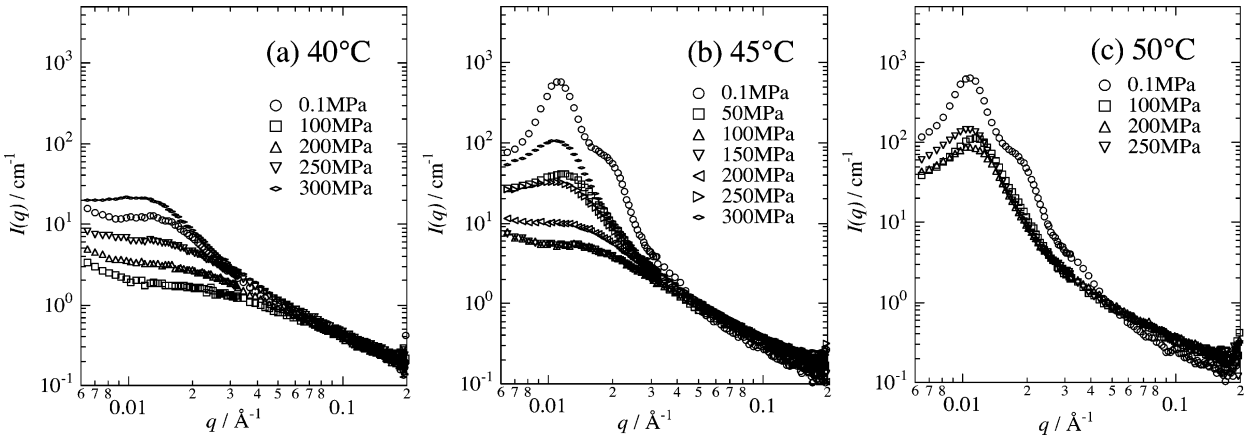

Figure 10. Pressure dependence of SANS intensity functions, $I(q)$s, of pEOEOVE-*b*-pMOVE in D_2O at (a) 40, (b) 45, and (c) 50 °C.

according to the following equation,

$$\xi = \xi_0 \left| \frac{P - P_{sp}}{P_{sp}} \right|^{-\nu_P} \tag{24}$$

where ν_P is the critical exponent for the pressure dependence of ξ, and P_{sp} is spinodal pressure. From the fit, we obtained $\nu_P = 0.61$, $P_{sp} = 350$ MPa and $\xi_0 = 8.49$ Å. The value of ξ_0 is on the order of the monomeric unit. Hence, the concentration fluctuations far away from the criticality are on the order of polymer segments, and the characteristic length of concentration fluctuations, i.e., ξ, diverges by approaching the spinodal line.

When a simple or binary fluid approaches the spinodal line, the fluid exhibits a critical phenomenon. Similarly, a three-dimensional Ising (3D Ising) type phenomenon was observed experimentally for polymer gels.[10,20] The value of the exponent observed in this work, 0.61, means that the phase separation is classified to the 3D Ising model and is close to that obtained with PNIPA aqueous solutions. Note that PNIPA aqueous solutions and gels are typical examples of hydrophobically solvated homopolymers and undergo both temperature- and pressure-induced phase separations. This divergence also means that the hydrophobically solvated block copolymer aqueous solutions phase separates macroscopically by pressurizing at low temperatures. In general, a different selective solvation of constituent block chains in a block copolymer solution causes microphase separation. However, the indication of macroscopic separation by pressurizing at low temperature does not distinguish a selective solvation. This suggests that the block copolymer can be treated as a homopolymer in this (P, T) region.

3.3. Pressure Dependence at high Temperature (45 °C). Figure 10 shows pressure dependence of SANS profiles for 15 wt % pEOEOVE-*b*-pMOVE in D_2O at (a) 40, (b) 45, and (c) 50 °C. At 40 °C, a broad peak was present at 0.1 MPa as shown by open circles. The peak decreased by increasing P up to 100 MPa. The SANS curve at 100 MPa is represented by the OZ equation and thus, it is considered that the block copolymers are dispersed in aqueous solution at 100 MPa. However, $I(q)$ reincreased by further increasing P. With further pressurizing, $I(q)$ became even higher than that at 0.1 MPa. This type of reentrant behavior of microphase separation is more clearly observed at 45 °C. Figure 10b shows that a bcc lattice structure of spherical micelles is formed at 45 °C under ambient pressure as is discussed in the previous section. Note that the reentrant behavior in $I(q)$ with respect to P is clearly observed. At 50 MPa, a suppression of the peak was observed and specific shoulder meaning the bcc lattice disappeared. At 100, 125, and 150 MPa, the peak disappeared, and the SANS curves were well fitted with the OZ equation. However, at 200 MPa, the SANS intensity increased, and an indication of microphase separation peak was detected at 250 MPa. The SANS curve at 300 MPa showed a further increase of the SANS intensity and a clear reappearance of microphase separation curve. In the case of 50 °C, on the other hand, $I(q)$ was not fully suppressed by pressurizing and remained in a microphase-separated state, and an intensity recovery was also observed as shown in Figure 10c. It is noteworthy that the shape of $I(q)$ in the high-pressure region, e.g., $P = 250$ and 300 MPa, is not the same as those in the low-pressure region. Hence, it is important to discuss whether the scattering peak observed at the high-pressure region has the same meaning or not.

We examined $I(q)$'s of the block copolymer solution at the high temperature and high-pressure regions with the following three different theoretical scattering functions, (a) the paracrystal model, (b) Leibler's correlation hole model,[38] and (c) Pedersen's micellar model.[39] The paracrystal model is the same as used in the analysis of $I(q)$ at ambient pressure as mentioned above. Leibler's model assumes that the block copolymer is in a disordered state near spinodal. The function is given by

$$I(q) \sim g_1(1,x)/\{g_1(f,x)g_1(1-f,x) - 0.25[g_1(1,x) - g_1(f,x) - g_1(1-f,x)]^2\} \tag{25}$$

where $g_1(f, x)$ is the Debye function for the block copolymer with the composition f and $x = q^2R_g^2$ with R_g denoting the radius of gyration of an ideal chain. The Pedersen's model assumes a scattering form factor for a block copolymer micelle with a spherical core, presence of corona chains attached to the core surface, and a hard-sphere structure factor. The total coherent scattering intensity can be expressed as

$$I(q) = P_{mic}(q) + A_{mic}(q)^2[S(q) - 1] \tag{26}$$

where $P_{mic}(q)$ is the micelle form factor, $A_{mic}(q)$ is the form factor amplitude of the radial scattering length distribution of the micelle, and $S(q)$ is the monodisperse hard-sphere structure factor.[39,40] The results of curve fittings for $P = 300$ MPa are displayed in Figure 11. The fitting parameters are as follows: paracrystal, $a = 690$ Å, $\Delta a/a = 0.23$, $R = 200$ Å, $\Delta R/R = 0.31$; Leibler, $R_g = 190$ Å, $f = 0.333$, Flory's interaction parameter $\chi = 0.020$; Pedersen, the number of polymer chains per micelle = 3.5, the volume fraction of micelles = 0.254, the hard-sphere radius for the structure factor = 257 Å, the radius of gyration of corona = 125 Å, the core-radius = 119 Å, the width of the interface = 62.0 Å, and the width parameter = 39.0 Å. Although all of the functions seem to well reproduce

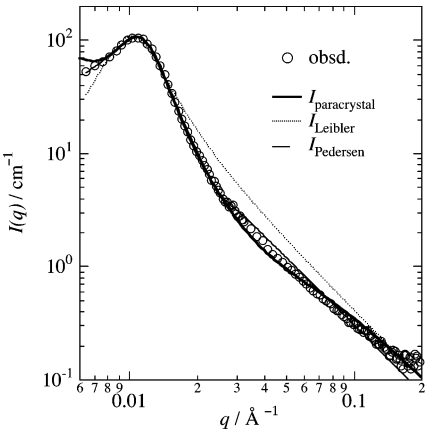

Figure 11. Comparison of the curve fitting of $I(q)$s for pEOEOVE-*b*-pMOVE in D_2O at 300 MPa with (a) paracrystal theory, (b) Leibler's theory, and (c) Pedersen's model.

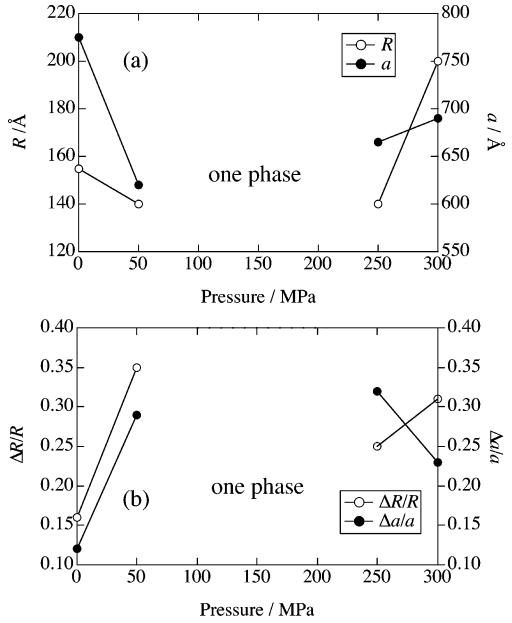

Figure 12. Pressure dependence of (a) the average radius of pEOEOVE core, R, and the average unit cell distance, a, and (b) their distributions, $\Delta R/R$ and $\Delta a/a$, at 45 °C.

the experimental scattering function except for the Leibler model, the physical meaning of the fitting parameters of Pedersen's models do not well represent the system under investigation. Hence, we employ the paracrystal theory to determine the microphase-separated structure at high pressures. This result indicates that block copolymer aqueous solutions undergo micelle formation followed by a bcc lattice formation even at high pressures.

Figure 12 shows the pressure dependence of (a) the average radius of pEOEOVE core, R, and the average unit cell distance, a, and (b) their distribution, $\Delta R/R$ and $\Delta a/a$ ($= g$), evaluated for the polymer solution at 45 °C with the paracrystal theory. The average radius of pEOEOVE core, R, at 300 MPa is larger than that at 0.1 MPa and it is considered that this is due to distorted micelles at high pressure. With regard to the average unit cell distance, a, the value at 300 MPa is smaller than that at 0.1 MPa. It is shown that the distributions, $\Delta R/R$ and $\Delta a/a$, at 300 MPa are larger than those at 0.1 MPa and this result obviously supports that the micelles and the bcc lattice are more distorted than those at 0.1 MPa.

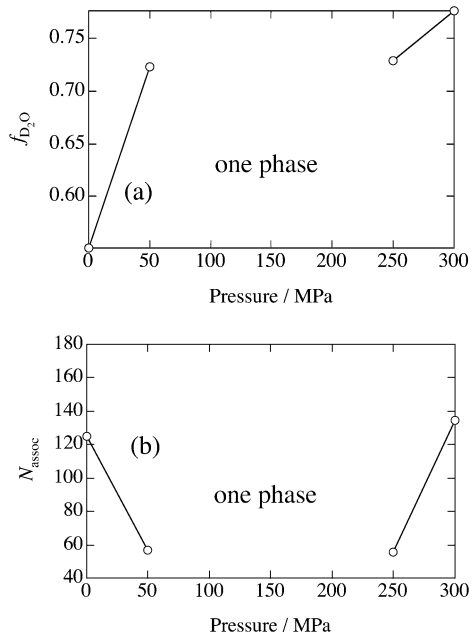

Figure 13. Pressure dependence of (a) the solvent fraction in the core, f_{D_2O} and (b) the number of polymer chains associated in a micelle core, N_{assoc}, for the system at 45 °C.

Let us discuss the physical implication of the pressure dependence of these structure parameters. The volume fraction of the solvent in the core, f_{D_2O}, and the number of polymer chains associated with a micelle, N_{assoc}, can be estimated by

$$f_{D_2O} = 1 - \frac{(\rho_{MOVE} - \rho_{D_2O})f_{MOVE} - \sqrt{\frac{I(0)a^3}{2V_{obs}^2}}}{(\rho_{EOEOVE} - \rho_{D_2O})} \quad (27)$$

$$N_{assoc} = \frac{V_{obs}f_{EOEOVE}N_{Av}}{M_{EOEOVE}/d_{EOEOVE}} \quad (28)$$

where ρ_{MOVE}, ρ_{EOEOVE}, and ρ_{D_2O} are scattering length densities for pMOVE, pEOEOVE, and D_2O, respectively. f_{MOVE} is the volume fraction of pMOVE in the micellar core. $I(0)$, V_{obs}, and N_{Av} are the scattering intensity at $q = 0$ and the volume of the micelle given by $4\pi R^3/3$, and the Avogadro number, respectively. M_{EOEOVE}, d_{EOEOVE}, and f_{EOEOVE}, are the monomer molecular weight, the mass density, and the volume fraction of pEOEOVE, respectively. Figure 13 shows the variation of f_{D_2O} and N_{assoc} at 45 °C as a function of P. Note that the system is in a disordered state in the middle pressure region, where f_{D_2O} and N_{assoc} were not evaluated. The value of f_{D_2O} increases by pressurizing. This indicates that the miscibility of pEOEOVE increases with increasing P. On the other hand, N_{assoc} decreases by increasing P up to 50 MPa, and recovers a similar value at 300 MPa. This readily leads to the following statements that the degree of selective solvation is suppressed at the high-pressure region.

The hypothesis of symmetric phase diagram suggests an appearance of similar SANS profiles with respect to $P_0 = 153.3$ MPa. However, the SANS intensity at 300 MPa (300 MPa $- P_0 = 146.7$ MPa) is not so strong as that at 0.1 MPa ($P_0 - 0.1$ MPa $= 153.2$ MPa). Seemingly, this means that the microphase separation at high pressure is not driven by strong hydrophobic interaction as is observed at ambient pressure. This result is consistent with the DLS results, where the gradual change of the block copolymers was observed at high pressure.

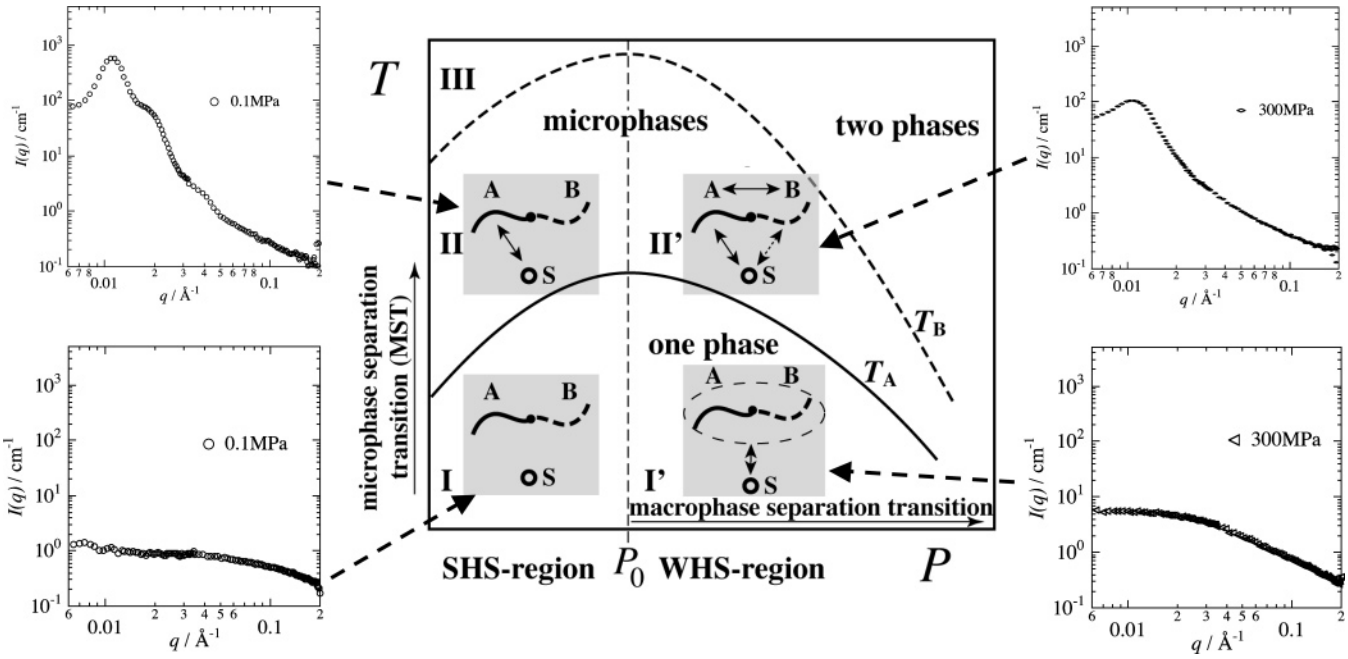

Figure 14. Phase diagram for pEOEOVE-*b*-pMOVE in D_2O at various pressures and temperatures. A, B, and S denote the A-block (pEOEOVE), B-block (pMOVE), and the solvent, respectively. The solid and dashed curves denote the microphase separation temperature curve, T_A(EOEOVE), and the precipitation temperature curve, T_B(MOVE). The symmetric pressure P_0 divides the strongly hydrophobic solvated (SHS) and the weakly hydrophobic solvated regions (WHS). The arrows indicate repulsive interaction, or selectivity solvation. The corresponding SANS intensity curves are also shown.

4. Selective Solvation at Various Pressures and Temperatures. In this section, we discuss "selective solvation" observed in pEOEOVE-*b*-pMOVE aqueous solutions at various pressures and temperatures in detail. A schematic picture of the interaction is shown in Figure 14.

Region I ($P \ll P_0$, $T < T_A$): It is shown that the scattering curves of the block copolymer aqueous solutions are well fitted with an OZ function. The correlation length is so small that the block copolymers are regarded to be well dispersed in aqueous solution.

Region I′ ($P > P_0$, $T < T_A$): At high pressure and at low temperatures, it is also shown that the scattering curves of the block copolymer aqueous solution are well fitted with OZ functions. However, the correlation length shows a critical phenomenon by pressurizing. These results mean that the block copolymers behave as homopolymers. This is ascribed to the solvent selectivity of the constituent block chains becoming insignificant by pressurizing.

Region II ($P \ll P_0$, $T > T_A$): At ambient pressure and at high temperatures, the block copolymers form a distinct bcc lattice of spherical micelles at nearly 40 °C by increasing temperature. In this case, EOEOVE segments are strongly associated and microphase separation takes place.

Region II′ ($P > P_0$, $T > T_A$): At high pressures and at high temperatures, the fitting results show that the block copolymers again form a bcc lattice of spherical micelles by further pressurizing. In addition, the selective solvation is not as strong as that at low pressures, which is consistent with the gradual change of the peak of the decay-rate distribution function at high pressure.

Region III ($T > T_B$): By increasing temperature above MOVE phase separation temperature, iceberg structure surrounding pzMOVE coronas is destroyed and the micelles are destabilized. In this case, the micelles aggregate and accordingly precipitation takes place.

Conclusion

Various types of phase separations induced by temperature and/or hydrostatic pressure were investigated for pEOEOVE-*b*-pMOVE aqueous solution, where both pEOEOVE and pMOVE were the thermosensitive hydrophobically solvated polymers. The SANS intensity functions as well as DSC and DLS results disclosed the following facts. (1) By increasing temperature under atmospheric pressure, a series of scattering peaks appeared in SANS intensity curves at about 40 °C, indicating microphase separation with pEOEOVE domains in a bcc packing in the matrix of pMOVE and water. The size of unit cell is about 775 Å, in which ca. 155 Å radius spherical domains are packed. Further increase of T resulted in a precipitation of the polymer at about 65 °C. This is due to demixing of the second blocks, i.e., pMOVE from water. (2) A pressure−temperature ($P-T$) phase diagram for microphase separation was determined by DLS for the first time. At a low pressure, a sudden decrease of the initial value of the intensity−intensity−time correlation function, $g^{(2)}(\tau) - 1$, was observed as a result of microphase separation. On the other hand, at high-pressure regions, such a depression is not observed. However, by increasing temperature, a fast-mode peak appeared in the decay-rate distribution function, $G(\Gamma)$. It seems reasonable that the appearance of this peak is related to the structural change of the block copolymer induced by phase separation. The resultant phase diagram is a convex-upward function. The phase diagram was fitted with an ellipse function having the center, $(P_0, T_0) = (153.3\ \text{MPa}, -12.3\ °\text{C})$. The phase behavior seemed to be symmetric with an axis of $P_0 \approx 150$ MPa. (3) Pressurizing of the polymer solution at ambient temperature resulted in a divergence of the correlation length. This was confirmed to be due to pressure-induced macrophase separation. The critical exponent was evaluated to be 0.61, close to the one obtained for temperature-induced phase transitions. This transition may be classified to three-dimensional Ising-type critical phenomena. (4) Unlike a pressure-induced transition at the ambient temper-

ature, the solution underwent a reentrant microphase dissolution-separation transition with increasing P at 45 °C. The SANS peaks disappeared and the intensity decreased at 100 MPa. Then, by further increasing P, the SANS intensity increased accompanying a scattering maximum. This reentrant microphase separation at high pressure was found to be different from one at low pressures.

It is naively expected that an increase in pressure has the same effect as that of a decrease of temperature. A typical example is a van der Waals gas undergoing condensation transition. Such kind of "corresponding state" relationship is also found in multicomponent systems, e.g., a mixture of surfactant, water, and oil.[41] In our study, however, a distinctly different phase behavior was observed in pEOEOVE-*b*-pMOVE aqueous solutions. That is, various types of phase transitions take place without a simple correlation between P and T, i.e., a macrophase separation at high pressures and microphase separation at high-temperature regions.

These findings lead to a conclusion that selectivity of hydrophobic solvation is suppressed at high pressures. In another word, the hydrophobic solvation is exclusively important in the low-pressure region. That is, polymer chains are "hydrophobically solvated" by iceberg formation in region I, and a microphase separation takes place due to the strong hydrophobic interaction at $T > T_A$, leading to a "selectively solvated region" (region II). Presence of hetero-segments in a block copolymer or in a protein plays a significant role in structure formation and in phase transitions in aqueous systems, such as protein folding, coil−globule transition, and volume-phase transition of gels. At $P > P_0$ (region I′ or II′), on the other hand, such a variety of structures cannot appear because hydrophobic hydration is not efficient.

Acknowledgment. This work was partially supported by the Ministry of Education, Science, Sports and Culture, Japan (Grant-in-Aid, 14045216 and 16350120)). The SANS experiment was performed with the approval of Institute for Solid State Physics, The University of Tokyo (Proposal Nos. 04.041, 04.221), at Japan Atomic Energy Agency, Tokai, Japan.

References and Notes

(1) Molau, G. E. In *Block Polymers*; Aggarwal, S. L., Ed.; Plenum Press: New York, 1970.
(2) Helfand, E.; Wasserman, Z. R. In *Developments in Block Copolymers*; Goodman, I., Ed.; Applied Science: New York, 1982.
(3) Hamley, I. W. *The Physics of Block Copolymers.* Oxford University Press: Oxford, 1998.
(4) Frielinghaus, H.; Schwahn, D.; Mortensen, K.; Almdal, K.; Springer, T. *Macromolecules* **1996**, *29*, 3263−3271.
(5) Steinhoff, B.; Rullmann, M.; Wenzel, M.; Junker, M.; Alig, I.; Oser, R.; Stuhn, B.; Meier, G.; Diat, O.; Bosecke, P.; Stanley, H. B. *Macromolecules* **1998**, *31*, 36−40.
(6) Schwahn, D.; Frielinghaus, H.; Mortensen, K.; Almdal, K. *Macromolecules* **2001**, *34*, 1694−1706.
(7) Frank, H. S.; Evans, M. W. *J. Chem. Phys.* **1945**, *13*, 507−532.
(8) Kauzmann, W. *Adv. Protein Chem.* **1959**, *14*, 1.
(9) Ben-Naim, A. *Hydrophobic Interaction.* Plenum Press: New York, 1980.
(10) Shibayama, M.; Isono, K.; Okabe, S.; Karino, T.; Nagao, M. *Macromolecules* **2004**, 37, 2909−2918.
(11) Nasimova, I. R.; Karino, T.; Okabe, S.; Nagao, M.; Shibayama, M. *Macromolecules* **2004**, *37*, 8721−8729.
(12) Nasimova, I. R.; Karino, T.; Okabe, S.; Nagao, M.; Shibayama, M. *J. Chem. Phys.* **2004**, *121*, 9708−9715.
(13) Osaka, N.; Shibayama, M. *Phys. Rev. Lett.* **2006**, *96*, 048303.
(14) Siegert, A. F. J. *MIT Radiat. Rep.* **1943**, 465.
(15) Martin, J. E.; Wilcoxon, J. *Phys. Rev. Lett.* **1988**, *61*, 373.
(16) de Gennes, P. G. *Scaling Concepts in Polymer Physics*; Cornell University: Ithaca, NY, 1979.
(17) Shibayama, M.; Hashimoto, T.; Kawai, H. *Macromolecules* **1983**, *16*, 16−28.
(18) Hosemann, R.; Bagchi, S. N. *Direct Analysis of Diffraction by Matter*; North-Holland: Amsterdam, 1962.
(19) Sugihara, S.; Kanaoka, S.; Aoshima, S. *Macromolecules* **2005**, *38*, 1919−1927.
(20) Shibayama, M.; Tanaka, T.; Han, C. C. *J. Chem. Phys.* **1992**, *97*, 6829−6841.
(21) Provencher, S. W. *Comput. Phys. Comm.* **1982**, *27*, 213−227.
(22) Matsumoto, M.; Murakoshi, K.; Wada, Y.; Yanagida, S. *Chem. Lett.* **2000**, 938.
(23) Okabe, S.; Nagao, M.; Karino, T.; Watanabe, S.; Shibayama, M. *J. Appl. Crystallogr.* **2005**, *38*, 1035−1037.
(24) Shibayama, M.; Nagao, M.; Okabe, S.; Karino, T. *J. Phys. Soc. Jpn.* 2005, *74*, 2728−2736.
(25) Shibayama, M.; Morimoto, M.; Nomura, S. *Macromolecules* **1994**, *27*, 5060−5066.
(26) Shibayama, M.; Mizutani, S.; Nomura, S. *Macromolecules* **1996**, *29*, 2019−2024.
(27) Schild, H. G. *Prog. Polym. Sci.* **1992**, *17*, 163.
(28) Brown, W.; Nicolai, T. *Colloid Polym. Sci.* **1990**, *268*, 977−990.
(29) Doi, M.; Edwards, S. F. *The Theory of Polymer Dynamics.* Oxford University Press: Oxford, U.K., 1986.
(30) Yuan, G.; Wang, X.; Han, C. C.; Wu, C. *Macromolecules* **2006**, *39*, 3642−3647.
(31) Okabe, S.; Sugihara, S.; Aoshima, S.; Shibayama, M. *Macromolecules* **2002**, *35*, 8139−8146.
(32) Brown, W.; Nicolai, T.; Dynamic properties of polymer solutions. In *Dynamic Light Scattering*; Brown, W., Ed. Clarendon: Oxford, U.K., 1993; pp 272−318.
(33) Hawley, S. A. *Biochemistry* **1971**, *10*, 2436.
(34) Smeller, L. *Biochim. Biophys. Acta* **2002**, *1595*, 11.
(35) Kunugi, S.; Tanaka, N. *Biochim. Biophys. Acta* **2002**, *1595*, 329.
(36) Fuse, C.; Okabe, S.; Sugihara, S.; Aoshima, S.; Shibayama, M. *Macromolecules* **2004**, *37*, 7791−7798.
(37) Shibayama, M.; Okabe, S.; Nagao, M.; Sugihara, S.; Aoshima, S.; Harada, T.; Matsuoka, H. *Macromol. Res.* **2002**, *44*, 311.
(38) Leibler, L. *Macromolecules* **1980**, *13*, 1602−1617.
(39) Pedersen, J. S. *J. Chem. Phys.* **2001**, *114*, 2839−2846.
(40) Bang, J.; Viswanathan, K.; Lodge, T. P. *J. Chem. Phys.* **2004**, *121*, 11489−11500.
(41) Seto, H.; Okuhara, D.; Kawabata, Y.; Takeda, T.; Nagao, M.; Suzuki, J.; Kamikubo, H.; Amemiya, Y. *J. Chem. Phys.* **2000**, *112*, 10608.

MA060723O